Thermal Transport in Cadmium Sulfide Nanocrystals and Magic-sized Clusters

by

Ming-Hsien Sun

A Thesis Presented in Partial Fulfillment
of the Requirements for the Degree
Master of Science

Approved October 2022 by the
Graduate Supervisory Committee:

Robert Wang, Chair
Konrad Rykaczewski
Liping Wang

ARIZONA STATE UNIVERSITY

December 2022

ABSTRACT

The thermal conductivity of cadmium sulfide (CdS) colloidal nanocrystals (NCs) and magic-sized clusters (MSCs) have been investigated in this work. It is well documented in the literature that the thermal conductivity of colloidal nanocrystal assemblies decreases as diameter decreases. However, the extrapolation of this size dependence does not apply to magic-sized clusters. Magic-sized clusters have an anomalously high thermal conductivity relative to the extrapolated size-dependence trend line for the colloidal nanocrystals. This anomalously high thermal conductivity could probably result from the monodispersity of magic-sized clusters. To support this conjecture, a method of deliberately eliminating the monodispersity of MSCs by mixing them with colloidal nanocrystals was performed. Experiment results showed that mixtures of nanocrystals and MSCs have a lower thermal conductivity that falls approximately on the extrapolated trendline for colloidal nanocrystal thermal conductivity as a function of size.

ACKNOWLEDGMENTS

First, I would like to express my sincere gratitude and appreciation to my advisor Dr. Robert Wang for offering me the opportunity to work in his Thermal Energy & Nanomaterials Lab for the past 2 years. He has trained me into an independent researcher with his great patience and experience during my master's journey. I've learned a lot from him not only on nanoscale energy transport, but more importantly how to organize ideas in academic writing and give a great presentation. Besides my advisor, I would also like to thank my committee members Dr. Liping Wang and Dr. Konrad Rykaczewski for their valuable advice and insightful comments on my thesis defense.

A huge thanks also goes to my wonderful labmates in ASU: Ashish Rana, Aastha Uppal, Najam Shah, Shreyas Kanetkar, and Yanan Zhang. I really learned a lot from them and those memories are meaningful in my life. I would especially like to thank my brother Ashish Rana for teaching me everything about nanocrystals and thermal conductivity measurement. His guidance and advice carried me through all the stages of this project. I really enjoyed the time we spent together in the lab and racquetball court.

Last but not least, I would like to thank my parents Hung-Chieh Sun and Ching-Hui Chang for their unconditional love and support throughout my entire life. Words can never express how grateful I am for everything they have done for me. Without their faith in me, I wouldn't be the person that I am today.

TABLE OF CONTENTS

Page

LIST OF TABLES

Table Page

LIST OF FIGURES

Figure Page

Figure Page

Figure Page

Figure Page

CHAPTER 1

INTRODUCTION AND BACKGROUND

1.1. Nanomaterials

Nanomaterials are a class of materials that have at least one dimension on the nanometer scale. According to quantum mechanics, energy carriers such as electrons and phonons are also material waves. When the dimension approach to de Broglie wavelength of the electron, the finite size of the system can influence the energy transport by altering the wave characteristics such as forming standing waves and creating new modes that do not exist in bulk materials. This energy quantization phenomenon is called quantum confinement (size) effect. Materials with such nanostructure exhibit unique optical, electronic, thermophysical, and mechanical properties, which has made them an interesting research target over the past few decades.

1.2. Colloidal Nanocrystals

Colloidal nanocrystals (NCs) are solution-grown, nanometer-sized particles, which consist of an inorganic crystalline core and an organic ligand shell bound to its surface.[1] These organic ligands mediate growth and nucleation of the nanocrystal by binding to its surfaces as a surfactant. Figure 1 demonstrates the atomic structure of a single nanocrystal with surface ligand shell. Typical ligands, such as carboxylates, amines, phosphonates, thiols, and halides, feature a head group that adheres to the nanocrystal surface and a hydrocarbon tail that helps stabilize the nanocrystal in the reaction mixture or purified dispersion. The ligand quantity, ligand binding group, and ligand length significantly impact the nanocrystal size, shape, crystal structure and stability. Nanocrystals with a size-tunable core exhibit unique physical properties owing to the quantum confinement effect. Numerous studies have shown that these emerging materials can be used in a wide variety of applications.

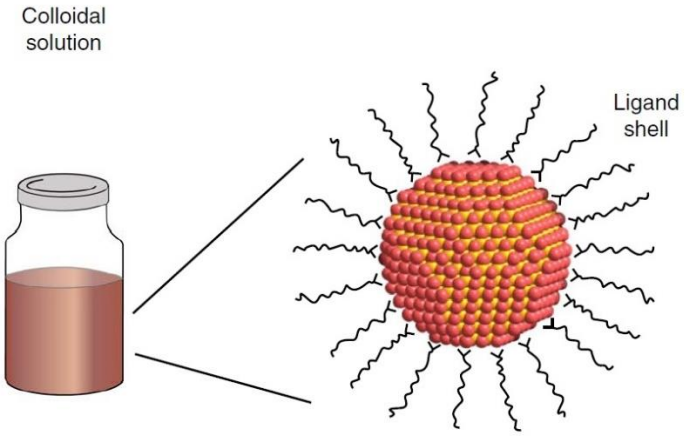

Figure 1 Schematic of colloidal nanocrystals with core and ligand shell. Reprinted with permission from Liu, M. et al., Colloidal Quantum Dot Electronics. Nature Electronics 4, 548-558 (2021). Copyright 2021 Springer Nature.

1.3. Magic-sized Cluster

Magic-sized Clusters (MSCs) are a class of ultrasmall (diameter < 2 nm) nanoparticles characterized by their identical (i.e., monodisperse) size and stoichiometry. Figure 2 shows a representative MSC for cadmium selenide ($Cd_{35}Se_{20}$) that is passivated by carboxylates and amines.[2] MSCs were recently discovered as intermediates during the nucleation and growth of semiconductor nanocrystals. Those clusters with precise number of atoms arrange in a close-shell configuration and structure that exhibits high thermodynamic stability. This characteristic results in the direct transition from one MSCs group to another without the appearance of any intermediate sizes. In the case of cadmium sulfide (CdS) MSCs, different cluster families (as defined by their first excitonic peak) have been reported previously in literature.[3] In this work, we will focus on the synthesis of CdS MSC-324 ($Cd_{37}S_{20}$ with exciton peak at 324 nm) and its corresponding thermal properties.

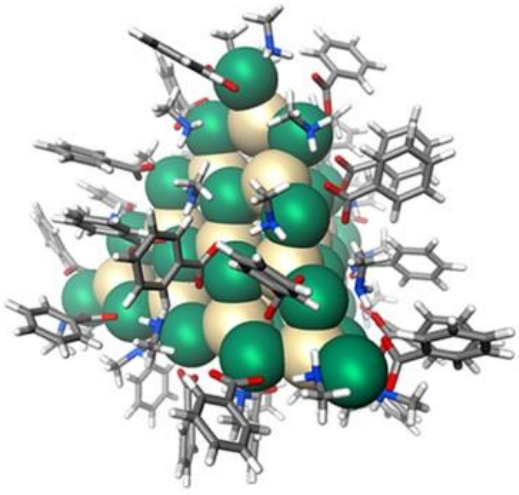

Figure 2 Relaxed structure of the $Cd_{35}Se_{20}$ cluster with all dangling bonds fully saturated by carboxylates and amines. Reprinted with permission from Voznyy, O. et al., Computational Study of Magic-Size CdSe Clusters with Complementary Passivation by Carboxylic and Amine Ligands. J. Phys. Chem. C, 120, 18, 10015-10019 (2016). Copyright 2016 American Chemical Society.

1.4. Thermal Transport in Colloidal Nanocrystals

Thermal transport in nanocrystals was first studied by Ong et al.[4] They reported the thermal conductivity measurements of nanocrystal arrays (NCAs) (CdSe, PbS, PbSe, PbTe, Fe_3O_4, and Au) and found a low value within the 0.1-0.3 $W/m^{-1}K^{-1}$ rage regardless of the core material. Molecular Dynamics (MD) simulations were also performed to compare with the experimental data (Figure 3a). The role of ligands in nanocrystal thermal transport was elucidated by exchanging long organic ligands (oleate, n-tetradecylphosphonate) with short inorganic ligands (N_2H_4, AsS_3^{3-}, $In_2Se_4^{2-}$) on PbS and CdSe. The thermal conductivities increased by 50% after ligand exchange (Figure 3b). All these measurement results indicate that thermal conductivities are insensitive to the core material, but strongly depend on the volume fractions of nanocrystal cores and surface ligands.

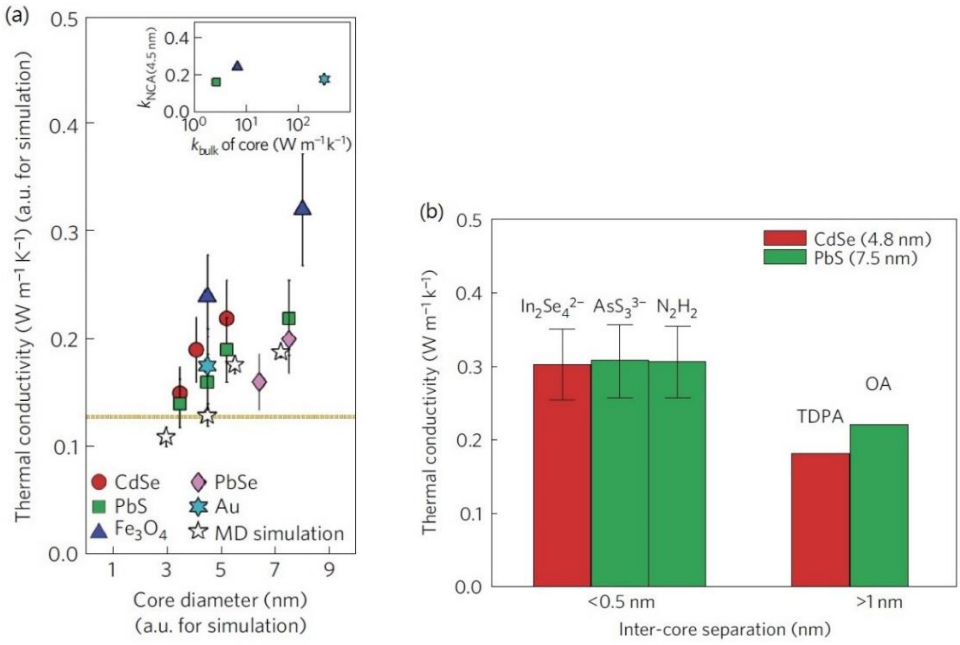

Figure 3 (a) Diameter series data for various NCAs have increasing thermal conductivity with core diameter regardless of core composition. (b) NCA thermal conductivity for different inorganic and organic ligands on CdSe and PbS nanocrystals. Reprinted with permission from Ong, W. et al., Surface Chemistry Mediates Thermal Transport in Three-dimensional Nanocrystal Arrays. Nature Materials 12, 410-415 (2013). Copyright 2016 Springer Nature.

Liu et al.[5] further reported a systematic study on how surface chemistry can affect the thermal transport in nanocrystal solids. They conducted several experiments using PbS NCs by varying core diameter (3.3-8.2 nm), ligand binding group (thiol, amine, atomic halides), and ligand length (ethanedithiol, butanedithiol, hexanedithiol, octanedithiol). The results agree with Ong's conclusions: (i) thermal conductivity of NC increases as the core diameter increases. (ii) Reducing the ligand length can decrease the interparticle distance, which increases thermal conductivity. Furthermore, Liu also found that the ligand binding strength to the NC core does not significantly impact thermal conductivity (Figure 4). By combining experimental observations with Effect Medium Approximation (EMA) modeling, they identified the ligand-ligand interface between neighboring NCs as a critical interface for heat transfer. Modifying this interface can boost thermal transport and thus will be beneficial to NC solid applications.

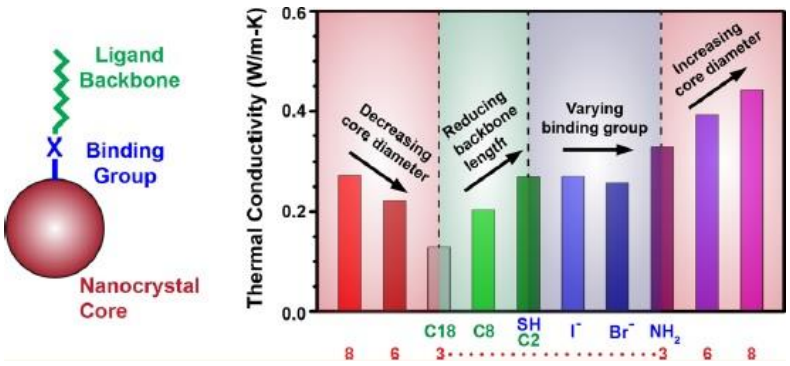

Figure 4 The effect of surface chemistry on thermal transport in colloidal nanocrystal (NC) solids: (1) increasing the NC diameter increases thermal conductivity. (2) Reducing the ligand length increases thermal conductivity. (3) The ligand binding strength to the NC core does not significantly impact thermal transport. Reprinted with permission from Liu, M. et al., Modifying Thermal Transport in Colloidal Nanocrystal Solids with Surface Chemistry. ACS Nano 9, 12079-12087 (2015). Copyright 2015 American Chemical Society.

Colloidal nanocrystals generally possess very low thermal conductivities. This phenomenon primarily results from the weak van der Waals interaction between ligands of adjacent nanocrystals. To overcome the thermal transport bottleneck, Wang et al.[6] reported a ligand crosslinking process which effectively exchange the weak van der Waals interaction with a strong covalent bond. They demonstrated the crosslinking process on iron oxide NCs with oleic acid (OA) ligand by heating the NC assembly to 350 °C for 30 minutes to split the C=C double bond of the OA molecule into saturated C-C single bonds that crosslinked adjacent ligands. The annealing process also causes a portion of the OA ligands to desorb and hence decreases the interparticle distance between the NCs. Figure shows the thermal conductivity measurement of non-crosslinked and cross-linked iron oxide NC solids as a function of core diameter at room temperature. The measurement results indicate that ligand crosslinking can yield a substantial increase in thermal conductivity of up to ~260 %.

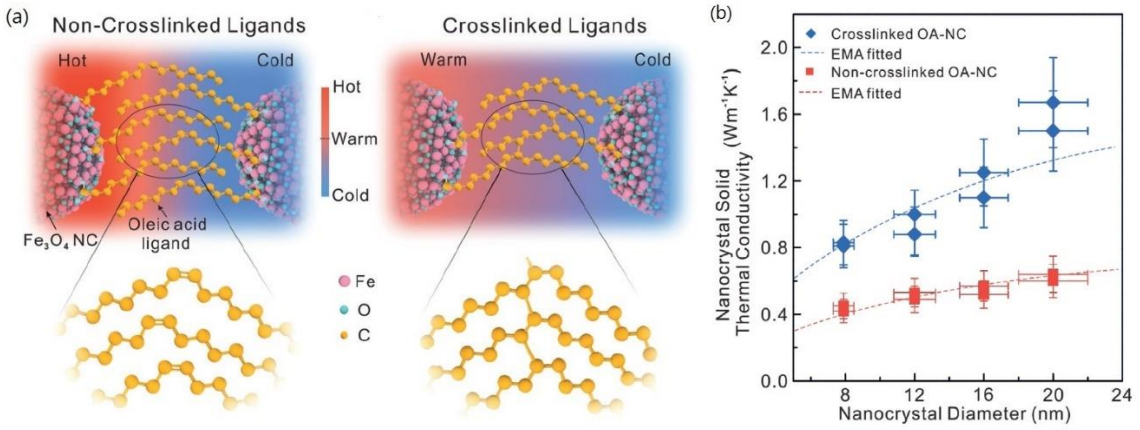

Figure 5 (a) Schematic illustration of ligand structure and the corresponding effect on thermal transport. The insets show zoomed-in views of the ligands before and after crosslinking. (b) Room-temperature thermal conductivity measurements on OA-capped iron oxide NC solids of different NC sizes before and after annealing at 350 °C. Reprinted with permission from Wang, Z. et al., Ligands Crosslinking Boosts Thermal Transport in Nanocrystal Solids. Angewandte Chemie - International Edition 59, 9556–9563 (2020). Copyright 2020 John Wiley and Sons.

Wang et al.[7] further reported thermal transport and mechanical measurements on single-domain colloidal PbS nanocrystal superlattices (NCSLs) that have long-range order as well as measurements on nanocrystal films (NCFs) that are comparatively disordered. Figure 6a shows the high-resolution SEM image of the disordered packing NCFs and ordered packing NCSLs. The NCSLs have better ligand interdigitation and alignment, which refers to the amount of overlap between the ligand shells of adjacent nanocrystals. Over an NC diameter range of 3-6.1 nm, the NCSLs show thermal conductivities and Young's moduli that are up to ~3 times higher than those of the corresponding NCFs. The measurements and computational modeling indicate that stronger ligand-ligand interactions due to enhanced ligand interdigitation and alignment in NCSLs account for the improved thermal transport and mechanical properties.

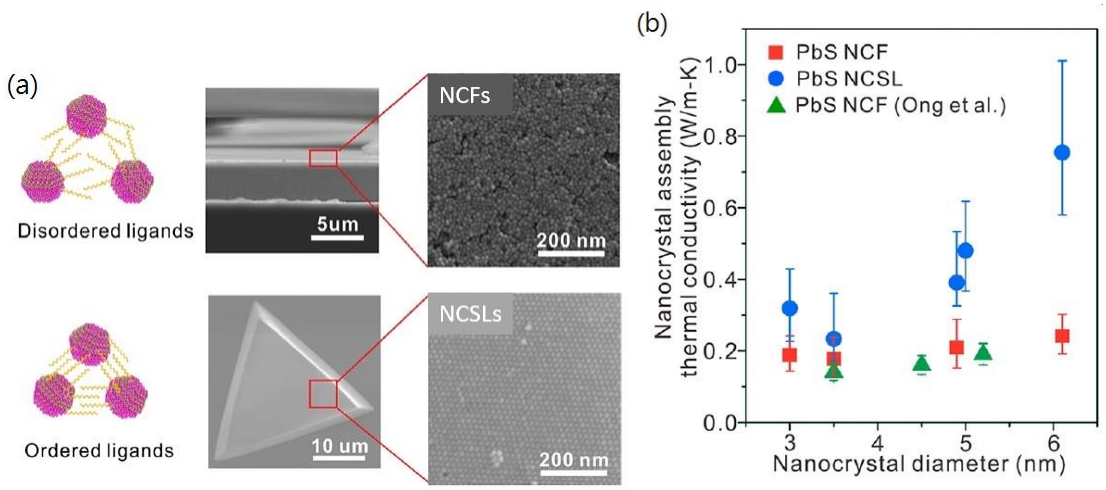

Figure 6 (a) Schematic of adjacent NCs and high-resolution SEM image of disordered ligand packing NCFs and ordered ligand packing NCSLs respectively. (b) Thermal conductivity of PbS NCSLs and NCFs of various core sizes. Reprinted with permission from Wang, Z. et al., Nanocrystal Ordering Enhances Thermal Transport and Mechanics in Single-domain Colloidal Nanocrystal Superlattices. Nano Letter 22, 4669-4676 (2022). Copyright 2022 American Chemical Society.

CHAPTER 2

MATERIAL SYNTHESIS AND CHARACTERIZATION

2.1. Colloidal Nanocrystals Synthesis

In a nanocrystal (NC) synthesis, the system consists of three components: molecular precursors, surfactants, and solvents. During synthesis, suitable molecular precursors are introduced into a reaction mixture, where they undergo a chemical reaction at a sufficiently high temperature. Precursors inside the reaction mixture decompose to form reactive atomic or molecular species called “monomers” (step I), which is followed by homogeneous nucleation (step II). Further growth occurs due to continuous flux of monomers onto the NC surface (step III). Upon depletion of the monomers, further growth may occur through Ostwald ripening, i.e., growth of larger dots by dissolving smaller ones. All these synthetic routes can be significantly altered by the presence of surfactant, also known as surface ligand or capping agent. These molecules dynamically adhere to the NC surface during NC nucleation and growth and provide chemical and colloidal stability of the final product.

It is generally accepted that temporally discrete nucleation and growth is required for growing monodisperse NCs. Temporally discrete nucleation is attained by the hot-injection technique, in which the precursors are rapidly injected into a hot solvent to induce an abrupt supersaturation of monomer. The concept of the nucleation “burst” relates to the fast nucleation that occurs after the monomer concentration surpasses a certain threshold, is originally proposed by La Mer et al.[8]

The synthesis recipe in this work is adapted from Peng et al.[9] They show that noncoordinating solvents not only are compatible with the synthesis of semiconductor nanocrystals, but also provide tunable reactivity of the monomers by simply varying the concentration of ligands in the solution. According to their results, the influence of the ligand concentration in controlling the size and size distribution of the nanocrystals is dramatic (Figure 7). The noncoordinating solvent used in this approach is octadecene (ODE), which is liquid at room temperature and boils at 320 °*C.* Oleic acid is used as the surface ligand for stabilizing the nanocrystals and the cationic precursors. Two precursors CdO and elemental sulfur were chosen as the Cd source and S source respectively. During the synthesis, a mixture of CdO, oleic acid, and ODE was heated to 300 °C. A solution of sulfur in ODE was swiftly injected into this hot solution, and the reaction mixture was allowed to tool to 250 °C for the growth of CdS nanocrystals. The whole synthesis is carried out under nitrogen.

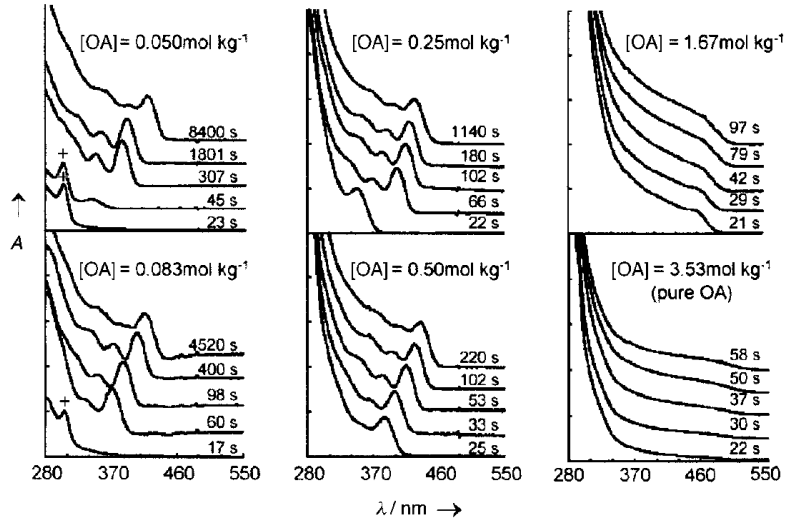

Figure 7 Temporal evolution of the absorption spectrum of the CdS nanocrystals grown in ODE with different oleic acid concentrations. The absorption peaks of a magic-sized nanocluster are marked +. A=Absorbance. Reprinted with permission from Yu, W. et al., Formation of High-quality CdS and other II-VI Semiconductor Nanocrystals in Noncoordinating Solvents: Tunable Reactivity of Monomers. Angewandte Chemie - International Edition 41, 2368–2371 (2002). Copyright 2002 John Wiley and Sons.

2.2. UV-Vis Spectroscopy and Photoluminescence

Nanoparticles exhibit unique optical properties highlighted by their tunable size, shape, surface characteristics and doping[10], which makes spectroscopy a valuable tool for studying and characterizing these materials. Nanoparticles made of semiconductor materials, often referred to as quantum dots (QDs), show a strong size dependency in absorption and photoluminescence spectrum due to quantum confinement effect. Moreels et al.[11] quantitatively investigated the size-dependent optical properties of colloidal lead sulfide (PbS) nanocrystals or QDs by combining the QDs absorbance spectra with detailed elemental analysis of the QDs suspension. A series of PbS QDs absorbance spectra in Figure 8a demonstrates that QDs band gap E_0, which relates to particle sizes, vary between 0.71 and 1.28 eV (1740 – 940 nm). The particle size is measured from the typical transmission electron microscope (TEM) image (Figure 8b, c) and correlated with E_0 to construct a sizing curve shown in Figure 8d. The experimental results and extrapolated sizing curve agree well with literature values presented by Cademartiri et al.[12], Borelli et al.[13], and Kane et al.[14]

The sizes of nanocrystals were determined either by TEM measurements or the sizing curves using their first absorption peak positions. The sizing curve of CdS shown in Figure 9 was reported by Yu. et al.[15] They combined the literature values and experimental measurement data to construct a sizing curve with an empirical fitting function.

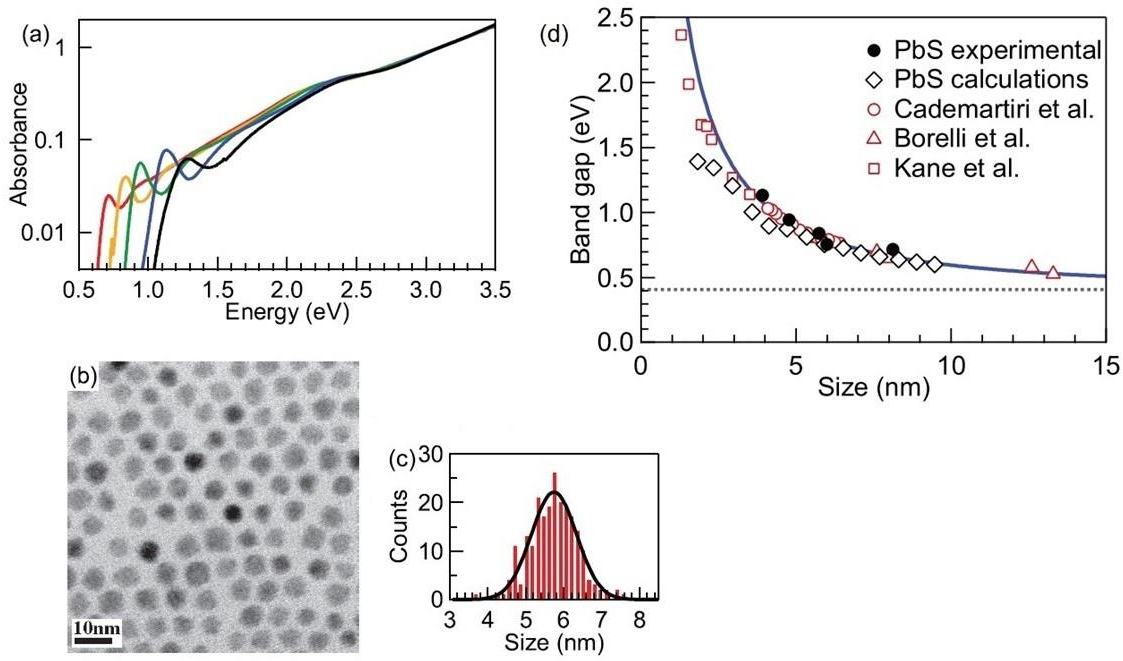

Figure 8 (a) Series of absorbance spectra of PbS QDs. (b) Overview TEM image of a typical PbS QDs. (c) Corresponding size histogram. The mean size equals 5.7 nm, with a size dispersion of 10% (d) Relation between the PbS QDs band gap and the particle size. To the set of experimental data, a sizing curve is fitted (full line). The dotted line denotes the bulk PbS band gap (0.41 eV). Reprinted with permission from Moreels, I. et al., Size-dependent Optical Properties of Colloidal PbS Quantum Dots. ACS Nano 3, 3023-3030 (2009). Copyright 2009 American Chemical Society.

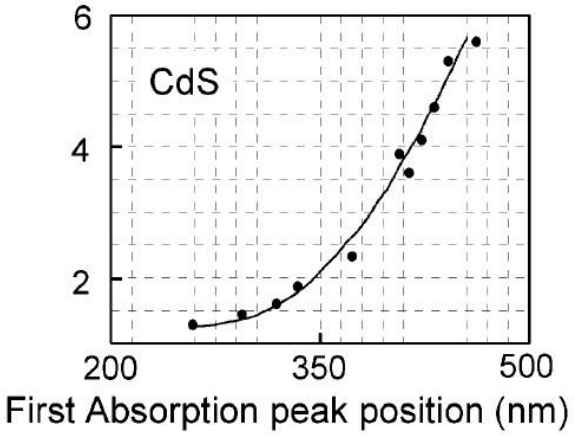

Figure 9 Sizing curve for CdS nanocrystals. Reprinted with permission from Yu, W. et al., Experimental Determination of the Extinction Coefficient of CdTe, CdSe, and CdS Nanocrystals. Chemistry of Materials, 15(14), 2854-2860 (2003). Copyright 2003 American Chemical Society.

CHAPTER 3

THERMAL CONDUCTIVITY MEASUREMENT

3.1. 3ω Method

The 3ω method is a widely used and well-established technique in measuring the thermal conductivity of thin film and bulk materials.[16] In general, a thin metal line being deposited on the thin film (or bulk material) functions both as a resistive heater and a resistance temperature detector (RTD). During measurement, the heater is driven with AC current oscillating at frequency ω, which induces periodic joule heating at frequency 2ω since the electrical resistance oscillates at 2ω. The heating at 2ω then causes the temperature of the line to oscillate at 2ω. This 2ω temperature oscillation then causes the electrical resistance to also oscillate at 2ω since the electrical resistance is linearly proportional to temperature in a metal. The 2ω oscillation in resistance (which carries the temperature information) multiplied by the 1ω current oscillation yields a 3ω voltage oscillation across the metal line. This 3ω voltage oscillation contains information in the sample's temperature change and is used to determine the thermal conductivity.

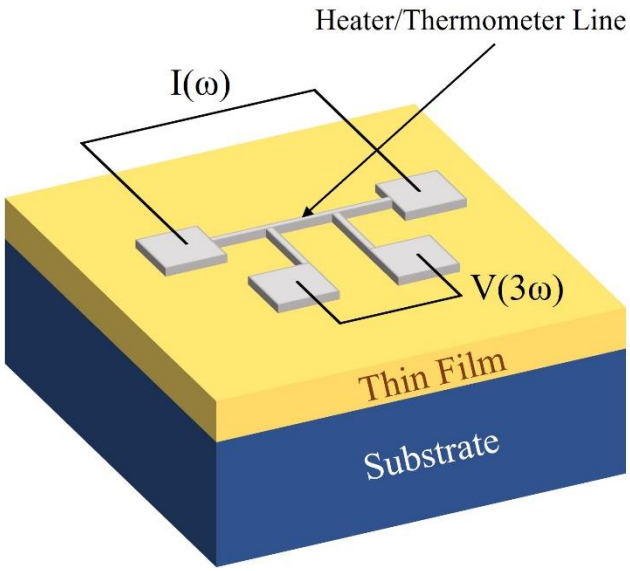

Figure 10 The geometry of the 3ω sample. A thin metal line with 4 electrodes is patterned onto the thin film. An electrical current of frequency ω is applied to the outside contacts. The 3ω voltage signal is measured at the inside contacts.

Our instrumentational closely follows the modified design from Feser[17]. A lock-in-amplifier (Stanford Research Systems, model SRS830) is used as the voltage source as well as the detector of the 3rd harmonic voltage signal, V(3ω). The voltage drives current through the sample's heater line, a potentiometer placed in series, and the internal resistance of the lock-in amplifier. A potentiometer is set to have a slightly larger electrical resistance (R_{pot}) than the sample's resistive heater and is determined before the experiment using a four-probe measurement from a digital multimeter. Prior to measurement, a small DC current is driven through the resistive heater and the potentiometer to determine the resistance of heater line (R_s) using the relation

$$R_s = R_{pot}\frac{V_{1\omega,s}}{V_{1\omega,pot}} \quad (1)$$

As Dames[18] has pointed out, there is a spurious current that travels through the circuit, which in turn creates an additional undesirable portion of the sample 3rd harmonic voltage signals. To solve this problem, instead of measuring $V_{3\omega,s}$ directly, we adjust the multiplying digital-to-analog converter so that the multiplying constant is $\alpha = \frac{R_s}{R_{pot}}$, and then measure the differential signal, $V_{3\omega,diff} = V_{3\omega,A-,V_{3\omega,B}}$. For each frequency, the temperature rises ΔT of the heater line can be determined by

$$\Delta T = 2R_s \frac{dT}{dR} \frac{V_{3\omega,diff}}{V_{1\omega,s}} \tag{2}$$

For room temperature measurements, the temperature coefficient of resistance ($TCR = \frac{1}{R_s}\frac{dR_s}{dT}$) is calibrated by measuring the temperature and 4-point resistance at 5 different temperatures between 20 *°C and 30 °C*, and a linear fit is used to determine the slope. The temperature rises in equation (1) is dissipated in the thin film and the substrate:

$$\Delta T = \Delta T_{film} + \Delta T_{sub} \tag{3}$$

If the frequency is chosen such that the thermal penetration depth into the substrate is much greater than the heater line width and film thickness, the temperature in the film, ΔT_{film}, will be frequency independent and temperature drop in the substrate, ΔT_{sub}, will be frequency dependent. If we measure the thermal response of the sample at two or more frequencies, we can extract the thermal conductivity of both the substrate and thin film. The substrate thermal conductivity can be calculated using

$$k_{sub} = \frac{V_{1\omega}^3 \ln\left(\frac{\omega_2}{\omega_1}\right)}{4\pi L R^2 (V_{3\omega} - V_{1\omega})} \frac{dR}{dT} \tag{4}$$

where L is the line length. To determine the thin film thermal conductivity, we first calculate the temperature drop in the substrate[19] as follows:

$$\Delta T_{sub} = \frac{P}{L\pi k_{sub}}\left[\frac{1}{2}\ln\left(\frac{k_{sub}}{(\rho c)(w/2)^2}\right) + 0.923 - \frac{1}{2}\ln(2\omega)\right] \quad (5)$$

Where P is the power dissipated by the heater line, w is the line width, ρ and c is the density and specific heat of the substrate respectively. The thermal conductivity of thin film can then be calculated using the following equation

$$k_{film} = \frac{P}{\Delta T_{film} wL} \quad (6)$$

3.2. Sample Preparation

The NCs and MSCs thin film were prepared by spin-coating the colloidal dispersion onto the 0.5 mm thick silicon wafer and then heating to 80° to remove residual organic solvent. A 3ω aluminum pattern (thickness ~ 150 nm) is deposited onto the film surface by electron-beam evaporation. Samples were then cut to a proper size and were connected to a 24-pin dual in-line package (DIP) using gold wire and silver conductive paste (SPI Silver Paste-Plus). A sample ready to be tested by the 3ω method is shown in Figure 11. During TCR measurement, the DIP was placed on a custom-built copper stage and thermoelectric module acting as a heat source. The temperature is recorded from a T-type thermocouple and read out using a thermocouple reader.

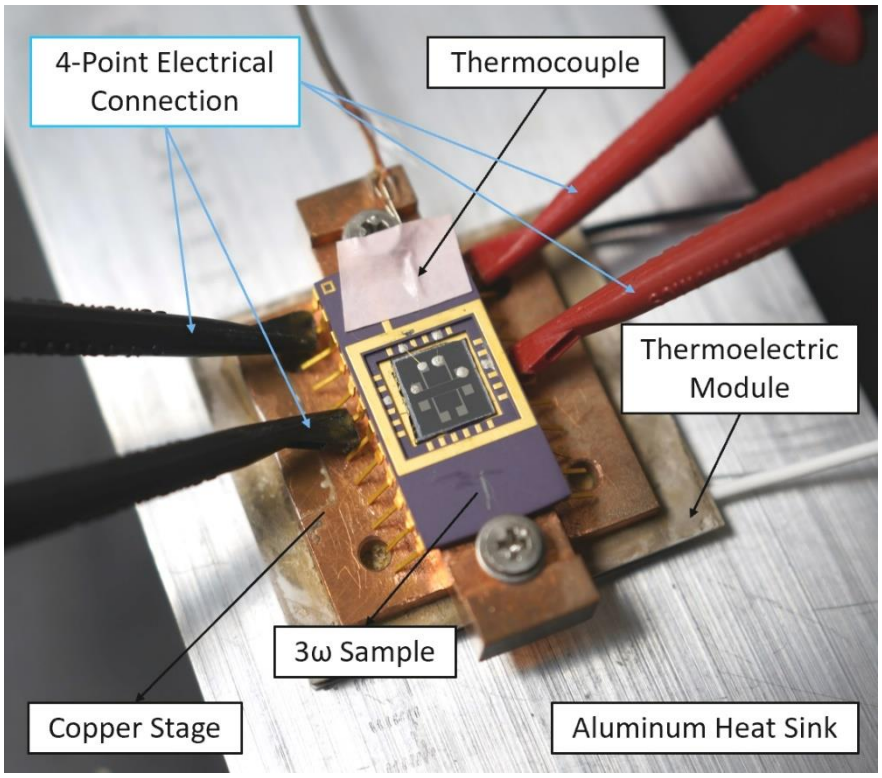

Figure 11 Custom-built stage for temperature coefficient of resistance (TCR) measurement.

3.3. Uncertainty Analysis

In order to design experiments with maximum accuracy, it is desirable to understand the most critical sources of error. The thermal conductivity of the samples, both the bulk materials as well as thin film samples, depend on several factors like film thickness, heater line dimensions, TCR, applied power, etc. Each of these parameters have an associated uncertainty which propagates through 3ω thermal conductivity calculation. The method used for uncertainty analysis and propagation is presented by Moffat[20] Let y be the final results and is a function of several measured variables (x_1, x_2, x_3, …, x_n) each with a corresponding bias uncertainty (B_{x1}, B_{x2}, B_{x3}, …, B_{xn}), an overall bias uncertainty is given by

$$B_y = \sqrt{\left(\frac{\partial y}{\partial x_1} B_{x1}\right)^2 + \left(\frac{\partial y}{\partial x_2} B_{x2}\right)^2 + \left(\frac{\partial y}{\partial x_3} B_{x3}\right)^2 + \cdots + \left(\frac{\partial y}{\partial x_n} B_{xn}\right)^2} \qquad (7)$$

The total uncertainty is a combination of the bias uncertainty and the precision uncertainty. Typically, the precision uncertainty can be calculated as follows

$$P_y = \sqrt{\left(\frac{\partial y}{\partial x_1} P_{x1}\right)^2 + \left(\frac{\partial y}{\partial x_2} P_{x2}\right)^2 + \left(\frac{\partial y}{\partial x_3} P_{x3}\right)^2 + \cdots + \left(\frac{\partial y}{\partial x_n} P_{xn}\right)^2} \qquad (8)$$

Where (P_{x1}, P_{x2}, P_{x3}, …, P_{xn}) are independent precision uncertainty. However, in this particular study, we found that the dominant precision uncertainty came from sample-to-sample variation (as opposed to statistical variation in any one x_n for a given measurement). Consequently, we used the sample-to-sample variation in thermal conductivity as our precision uncertainty. In addition, since the number of data points of our measurements are less than 30, the Student T distribution was used for estimating the precision uncertainty. For a data set (y_1, y_2, y_3, …, y_n), the precision uncertainty is given

$$P_y = t_{\alpha/2,v} \frac{S_y}{\sqrt{n}} \quad (95\%) \tag{9}$$

Where S_x is the standard deviation, and $t_{\alpha/2,v}$ is the t value corresponding to 95% confidence. The total uncertainty can then be determined from

$$U_y = \sqrt{{B_y}^2 + {P_y}^2} \tag{10}$$

Where B_x is bias uncertainty and P_x is precision uncertainty.

3.4. Calibration Samples

To calibrate our 3ω setup, four control samples have been measured and the results is summarized in

Table 1. Among these control samples, two of them are bulk materials (Si and GaAs) and the other two are thin film samples (SiO_2 and Al_2O_3) with thickness ~150 nm. Our results are in good agreement with the literature values.

Sample	**Sample Type**	**Line Dimensions (μm)**		**TCR (/°C)**	**Thermal Conductivity (W/mK)**	
		Length	**Width**		**Reference**	**Measured**
Si	Bulk	800	6	0.001721	142	142.09
GaAs	Bulk	500	5	0.001906	46	47.57
SiO_2	Thin film	2400	45	0.004128	1.3	1.69
Al_2O_3	Thin film	800	10	0.004234	1.6	1.57

Table 1 Thermal conductivity measurement of control samples using 3ω method.

CHAPTER 4

RESULTS AND DISCUSSION

We synthesized cadmium sulfide (CdS) NCs and MSCs based on the reported hot-injection method.[3,21]Both NCs and MSCs are capped with oleic acid (OA) as surface ligands. Different sizes of CdS NCs were obtained by varying the concentration of ligand in the solution. UV-Vis spectrometry techniques were used for material characterization. Since the quantum confinement effect is observable in NCs and MSCs, optical properties often serve as indicators that reflect the change in particle sizes. In Figure 12, we show the UV-Vis absorption spectra of as prepared nanocrystals and magic-sized cluster. The full width at half maximum (FWHM) of the PL spectrum or half width at half maximum (HWHM) of the absorption spectrum was used to reflect particle size distributions.[15]

Our CdS NCs possess sharp absorption peaks between 380-450 nm (FWHM ~ 24-40 nm), which are among the typical class of CdS NCs reported.[3,21] The MSC shows the absorption peak at 324 nm with a much narrower breadth (FWHM ~ 8 nm), which is similar to what has been reported for Cd-based MSCs.[3,22–24] The much narrower peak width of MSC-324 matches the one obtained in the reference.[3,24] The particle sizes were estimated by the empirical sizing curve presented by Yu et al.[15]They have used extinction coefficient to derive an empirical formula to relate the first absorption peak from the UV-Vis spectra to the corresponding size measured using TEM.

$$D = (-6.6521 \times 10^{-8})\lambda^3 + (1.9557 \times 10^{-4})\lambda^2 - (9.2352 \times 10^{-2})\lambda + 13.29 \quad (11)$$

In the above equation, D (nm) is the size of a given nanocrystal sample, and λ (nm) is the wavelength of the first excitonic absorption peak of the corresponding sample.

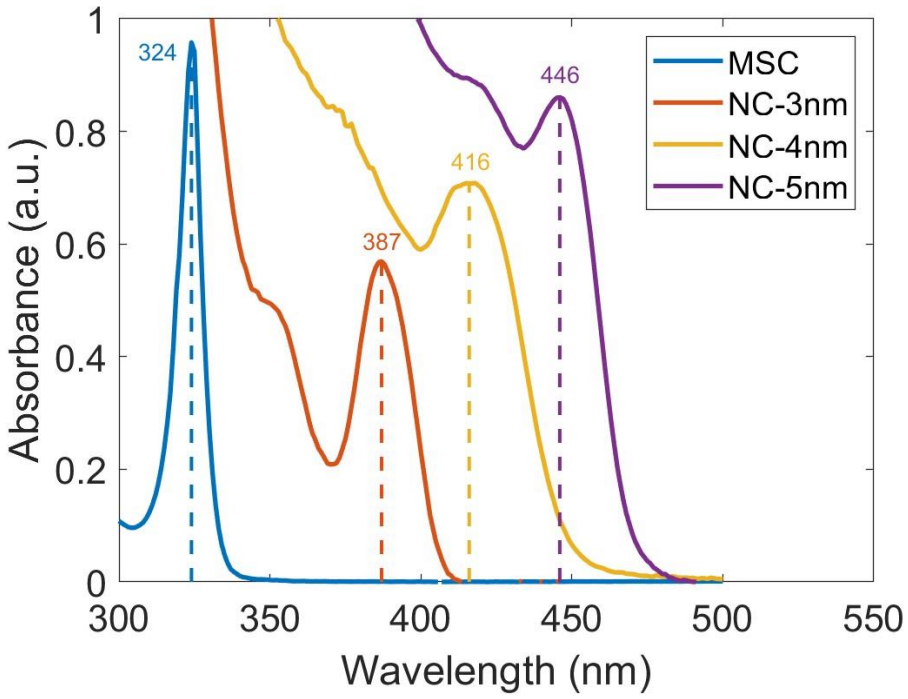

Figure 12 UV-Vis absorption spectrum of the CdS nanocrystals and magic-sized clusters (blue line) samples

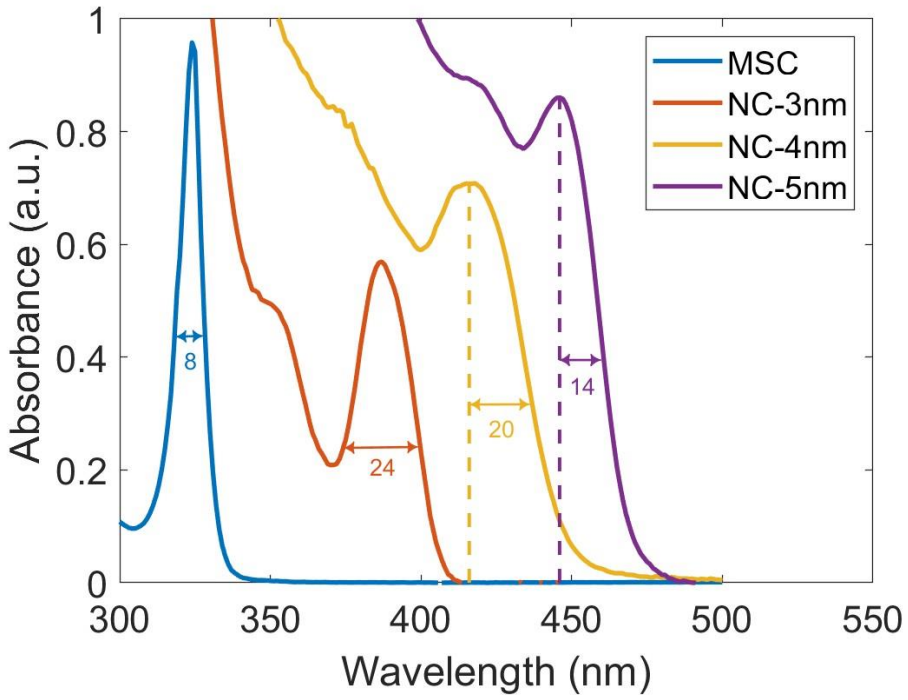

Figure 13 UV-Vis absorption spectrum of the CdS nanocrystals and magic-sized clusters (blue line) samples with their FWHM.

We first investigate the thermal conductivity of CdS NCs of different sizes. According to Ong's[4] results, thermal conductivities of semiconductor nanocrystal array are controllable within the range of 0.1-0.3 $Wm^{-1}K^{-1}$, and only weakly depend on the inorganic core material. Energy transport is mediated by the surface chemistry and the volume fractions of NC cores and surface ligand. The measured thermal conductivity as a function of core diameter for our as synthesized CdS NCs are shown in Figure 14 (blue data points). Thermal conductivity linearly increases as the core size increased from 3 nm to 5 nm. This trend of increasing thermal conductivity with increasing NC diameter is consistent with previous studies since the volume fraction of the NC core is increasing. Ong's[4] and Liu's[5] work shows that ligand matrix is a thermal insulating material compared to the nanocrystal core since ligand-ligand interface is characterized by weak van der Waals force. That is to say, the effect of ligand-ligand interactions contributes less to thermal conductivity as core size increases since the volume fraction of ligand matrix itself is reduced.

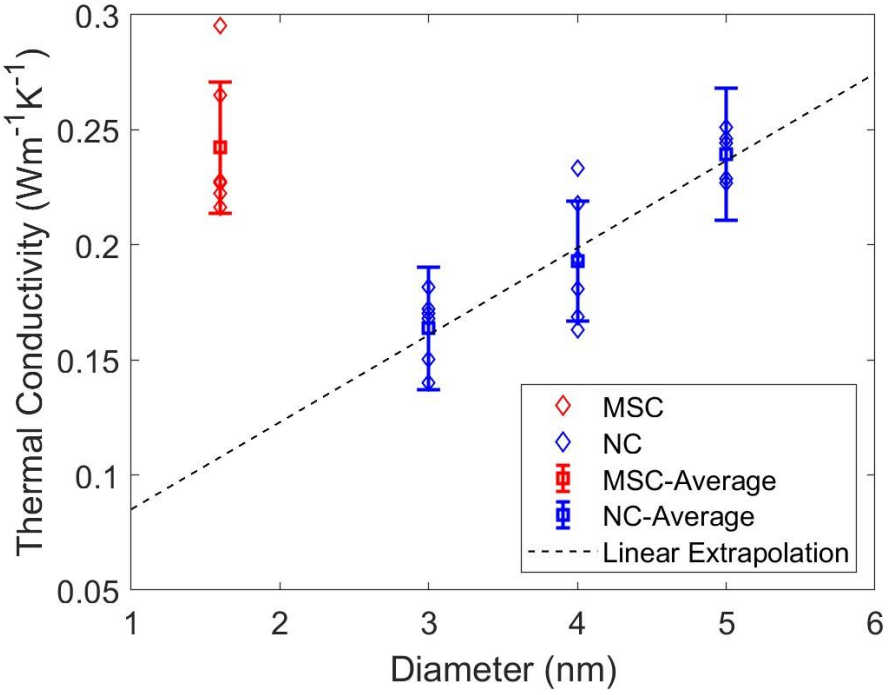

Figure 14 Thermal conductivity of CdS nanocrystals (blue data points) and magic-sized clusters (red data points) as the function of core size.

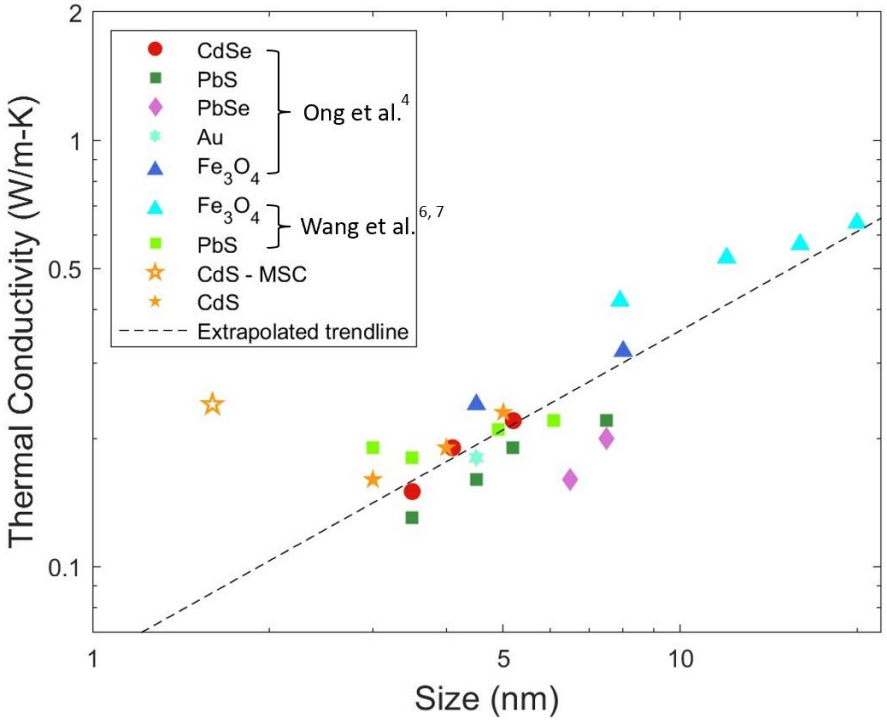

Figure 15 Thermal conductivity compilation of various nanocrystals of different sizes. CdS magic-sized clusters show an anomalously high value which is above the extrapolated trendline.

Since MSC molecules possess an exact stoichiometric composition and well-defined structure, it is an interesting class of nanomaterial with atomic level mono-dispersity. This unique feature results in a very sharp peak (FWHM ~ 8 nm) in absorption spectrum. To study the relative impact of monodispersity on thermal transport, the thermal conductivity of CdS MSC-324 was measured and plotted in the same figure (Figure 14 red data point). Our results show an average value of 0.25 $Wm^{-1}K^{-1}$, which is anomalously high considered its estimated size (~ 1.6 nm). We hypothesize this boost of thermal transport is due to the monodispersity (i.e., uniform size) and a potentially reduced interparticle distance. We use the term" ligand packing density" to refer to the amount of overlap between ligand shells of adjacent MSC molecules. We speculate that MSCs pack more uniformly and more closely together due to their perfect monodispersity. This improved packing leads to improved ligand-ligand interactions between adjacent particles and increased thermal transport. Even though the ligand-ligand interface still features weak van der Waals force, thermal transport in MSCs is improved by enhanced ligand packing density.

To gain further insight into the effect of monodispersity on thermal transport, we pursued a method of eliminating monodispersity by deliberately mixing 3 nm NCs and MSC-324 solution with each other at various weight percentages. This method is motivated by Abeles[25] in his study on thermal conductivity of a disordered silicon-germanium alloy as a function of compositions. Figure 16 shows the thermal conductivity of 3 nm NCs & MSC-324 mixture as a function of wt% of MSC. Whereas one might expect the thermal conductivity of mixtures to be an effective mean approximation of the two components, this is not the case for MSC-NC mixtures. Notably, the thermal conductivity is found to

drop sharply after a small amount of mixing and is below that of either the 100% NC case or the 100% MSC cases. In the range between 25% to 75%, the thermal conductivity is independent of composition. This result substantiates our conjecture that monodispersity of MSCs plays a critical role in thermal transport.

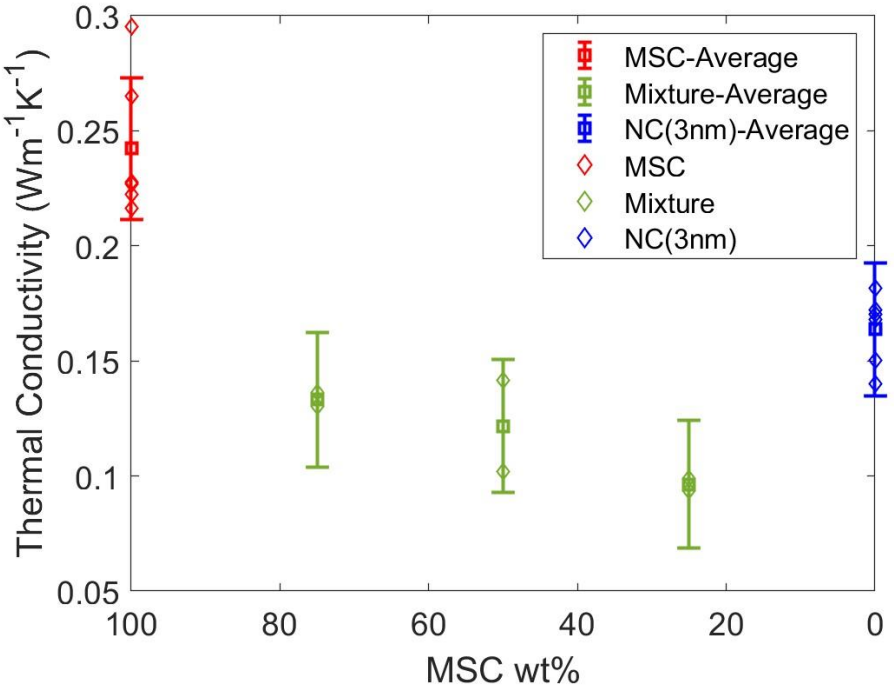

Figure 16 Thermal Conductivity of 3 nm nanocrystals and MSC-324 mixture at different weight percentage.

CHAPTER 5

CONCLUSION

In summary, we report that thermal conductivities of 3-5 nm CdS NCs fall in the range between 0.1-0.3 $Wm^{-1}K^{-1}$ and follow the trend that increasing the NC diameter increases thermal conductivity. The monodisperse CdS MSC-324, on the other hand, has an anomalously high thermal conductivity ~ 0.25 $Wm^{-1}K^{-1}$, which is close to that of 5 nm NC. Considering its ultrasmall size (~1.6 nm), this amount of increase can be attributed to the atomic-precise monodispersity and likely better ligand packing density. In order to better understand the effect of monodispersity on thermal transport, we present a way to eliminate monodispersity by mixing NCs and MSCs to yield size disorder and attenuated ligand-ligand interactions. The experimental results show that thermal conductivities are found to drop after adding a small perturbation and are independent of composition in the range of 25 – 75 wt%. This approach of creating size disorder further confirms that monodispersity plays an important role in boosting thermal transport of MSCs assemblies.

REFERENCES

1. Yin, Y. & Alivisatos, A. P. Colloidal nanocrystal synthesis and the organic-inorganic interface. *Nature* vol. 437 664–670 Preprint at https://doi.org/10.1038/nature04165 (2005).

2. Voznyy, O., Mokkath, J. H., Jain, A., Sargent, E. H. & Schwingenschlögl, U. Computational study of magic-size Cdse clusters with complementary passivation by carboxylic and amine ligands. *Journal of Physical Chemistry C* **120**, 10015–10019 (2016).

3. Nevers, D. R., Williamson, C. B., Hanrath, T. & Robinson, R. D. Surface chemistry of cadmium sulfide magic-sized clusters: a window into ligand-nanoparticle interactions. *Chemical Communications* **53**, 2866–2869 (2017).

4. Ong, W. L., Rupich, S. M., Talapin, D. v., McGaughey, A. J. H. & Malen, J. A. Surface chemistry mediates thermal transport in three-dimensional nanocrystal arrays. *Nat Mater* **12**, 410–415 (2013).

5. Liu, M., Ma, Y. & Wang, R. Y. Modifying Thermal Transport in Colloidal Nanocrystal Solids with Surface Chemistry. *ACS Nano* **9**, 12079–12087 (2015).

6. Wang, Z. *et al.* Ligand Crosslinking Boosts Thermal Transport in Colloidal Nanocrystal Solids. *Angewandte Chemie - International Edition* **59**, 9556–9563 (2020).

7. Wang, Z. *et al.* Nanocrystal Ordering Enhances Thermal Transport and Mechanics in Single-Domain Colloidal Nanocrystal Superlattices. *Nano Lett* **22**, 4669–4676 (2022).

8. Lamer, V. K. & Dinegar, R. H. *Theory, Production and Mechanism of Formation of Monodispersed Hydrosols*. https://pubs.acs.org/sharingguidelines.

9. Yu, W. W. & Peng, X. Formation of high-quality CdS and other II-VI semiconductor nanocrystals in noncoordinating solvents: Tunable reactivity of monomers. *Angewandte Chemie - International Edition* **41**, 2368–2371 (2002).

10. Zhang, J. *OPTICAL PROPERTIES AND SPECTROSCOPY OF NANOMATERIALS*.

11. Moreels, I. *et al.* Size-dependent optical properties of colloidal PbS quantum dots. *ACS Nano* **3**, 3023–3030 (2009).

12. Cademartiri, L. *et al.* Size-dependent extinction coefficients of PbS quantum dots. *J Am Chem Soc* **128**, 10337–10346 (2006).

13. Borrelli, N. F. & Smith, D. W. *Quantum confinement of PbS microcrystals in glass*. *Journal of Non-Crystalline Solids* vol. 180 (1994).

14. Kane, R. S., Cohen, R. E. & Silbey, R. *Theoretical Study of the Electronic Structure of PbS Nanoclusters*. https://pubs.acs.org/sharingguidelines (1996).

15. Yu, W. W., Qu, L., Guo, W. & Peng, X. Experimental determination of the extinction coefficient of CdTe, CdSe, and CdS nanocrystals. *Chemistry of Materials* **15**, 2854–2860 (2003).

16. Cahill, D. G. Thermal conductivity measurement from 30 to 750 K: The 3ω method. *Review of Scientific Instruments* **61**, 802–808 (1990).

17. Feser, J. P., Chan, E. M., Majumdar, A., Segalman, R. A. & Urban, J. J. Ultralow thermal conductivity in polycrystalline CdSe thin films with controlled grain size. *Nano Lett* **13**, 2122–2127 (2013).

18. Dames, C. & Chen, G. 1ω, 2ω, and 3ω methods for measurements of thermal properties. *Review of Scientific Instruments* **76**, 1–14 (2005).

19. Lee, S. M. & Cahill, D. G. Heat transport in thin dielectric films. *J Appl Phys* **81**, 2590–2595 (1997).

20. Moffat, R. J. *Describing the Uncertainties in Experimental Results*.

21. Peng, Z. A. & Peng, X. Formation of high-quality CdTe, CdSe, and CdS nanocrystals using CdO as precursor [6]. *Journal of the American Chemical Society* vol. 123 183–184 Preprint at https://doi.org/10.1021/ja003633m (2001).

22. Williamson, C. B. *et al. Chemically reversible isomerization of inorganic clusters Downloaded from*. http://science.sciencemag.org/ (2019).

23. Zhang, B. *et al.* Thermally-induced reversible structural isomerization in colloidal semiconductor CdS magic-size clusters. *Nat Commun* **9**, (2018).

24. Nevers, D. R. *et al.* Mesophase Formation Stabilizes High-Purity Magic-Sized Clusters. *J Am Chem Soc* **140**, 3652–3662 (2018).

25. Abeles, B. Lattice thermal conductivity of disordered semiconductor alloys at high temperatures. *Physical Review* **131**, 1906–1911 (1963).